Quasi-classical trajectory approach to the O(^{1}D)+HBr→OH+Br reaction stereo-dynamics on X^{1}A′ potential energy surface*

Li Hong(李 红), Zheng Bin(郑 斌), Yin Ji-Qing(尹吉庆), and Meng Qing-Tian(孟庆田)†

College of Physics and Electronics, Shandong Normal University, Jinan 250014, *China*

(Received 25 March 2011; revised manuscript received 4 May 2011)

The vector properties of reaction O(^{1}D)+HBr→OH+Br on the potential energy surface (PES) of X^{1}A′ ground singlet state are studied by using the quasi-classical trajectory (QCT) theory. The polarization-dependent differential cross sections (PDDCSs), the average rotational alignment factor $\langle P_2(\boldsymbol{j}' \cdot \boldsymbol{k})\rangle$, as well as the distributions reflecting vector correlations are also computed. The analysis of the results shows that the alignment and the orientation distribution of the rotation angular momentum vector of product molecule OH is influenced by both the effect of heavy–light–heavy (HLH) type mass combination and the deep well of PES.

Keywords: product polarization, O+HBr reaction, quasi-classical trajectory, vector correlation

PACS: 34.10.+x **DOI:** 10.1088/1674-1056/20/12/123401

1. Introduction

These days halogenated compounds have been widely studied due to their large abundance in nature and importance for environmental protection and human health.[1−7] In the stratosphere, HOBr is an important atmospheric species related to some photochemical and heterogeneous processes affecting the stratospheric ozone abundance.[8,9] In order to know the influence of the photolysis and the stability of HOBr on the catalytic removal of ozone in the atmosphere, several experimental studies have been carried out. The determination of the UV/visible absorption and the cross sections of HOBr are performed with some experiments.[10−15] Ruscic and Berkowitz[16] have successfully determined the heat of formation of HOBr and the dissociation energy of HOBr in experiment. Lock *et al.*[17] have employed the method of laser induced fluorescence combined with polarization and the effect of sub-Doppler spectroscopy to study the photodissociation dynamics of HOBr.

From a theoretical point of view, McGrath and Rowland[18] have used the Gaussian-2 theory to calculate the heat of formation of HOBr. Palmieri *et al.*[19] have derived the anharmonic near-equilibrium potential energy function of HOBr using the method of multireference configuration interaction wave function (MRCI) and a cc-PVTZ basis set.[20,21] The equilibrium structure, the harmonic frequency and the relative energy of HOBr have been computed by Lee *et al.*[22] through employing the coupled cluster method and a TZ2P basis set. Füsti–Molnar *et al.*[23] have computed the potential energy surfaces (PESs) for the three lowest lying singlet electronic states of HOBr, which provides the basic data needed to compute the dynamics of the HOBr+hν→OH+Br photodissociation process. An accurate global *ab initio* PES for this reaction, based on highly correlated coupled cluster singles and doubles with a perturbative triples (CCSD(T)) method and explicit basis set, was obtained by Peterson.[24]

The accurate global *ab initio* PES of HOBr encourages us to investigate its dynamics. In order to obtain an accurate theoretical description of the dynamics, we should have a more complete theoretical study. Recently, Tang *et al.*[25] have successfully employed the three-dimensional time-dependent wave packet method to study the scalar properties of the reaction such as initial state-selected reaction probability, reactive cross section and thermal rate constant. In addi-

*Project supported by the National Natural Science Foundation of China (Grant No. 11074151), the National Basic Research Program of China (Grant No. 2011CB808105), and the Open Fund of the State Key Laboratory of High Field Laser Physics (Shanghai Institute of Optics and Fine Mechanics).

†Corresponding author. E-mail: qtmeng@sdnu.edu.cn

© 2011 Chinese Physical Society and IOP Publishing Ltd

tion, Gogtas[26] has used the time-dependent quantum method to investigate the kinetics of the reaction of $O(^1D)$+HBr→OH+Br. However, to the best of our knowledge, there have been few quasi-classical trajectory (QCT) calculations to investigate the stereodynamics of the reaction of $O(^1D)$+HBr→OH+Br up to now. In this paper, therefore, we concentrate on the vector properties of the title reaction by using the QCT method. The remainder of this paper is organized as follows. The theory used is described in Section 2. The results and the discussion are given in Section 3. We conclude with a discussion of this work in Section 4.

2. Theory

In this paper, we employ the global analytical PES for the ground electronic state of HOBr, which is determined by Peterson using the method of highly correlated MRCI and an explicit basis set.[27] The *ab initio* data and analytical function form of the PES can be obtained in Ref. [28].

The calculation method we used in this study is the same as the one used in Refs. [29]–[38]. In our calculation, we integrate the classical Hamilton equations in three dimensions. Setting the initial rovibrational conditions of the HBr reagent to be $v = 0$ and $j = 0$, the collision energy is chosen from 0.24 eV to 1.0 eV for the properties of the PES of the title reaction. Each reaction runs 10000 trajectories and the integration step size is set as 0.1 fs for guaranteeing the conservations of total angular momentum and total energy.

We employ the standard theory of the product polarization established by Han *et al.*[30−34,39] However, here we just introduce the details related to our present work. In the centre-of-mass (CM) frame shown in Fig. 1, the relative velocity vector $\boldsymbol{k}'$ of the reactant is parallel to the z axis and the x–z plane is the scattering plane which contains the initial and the final relative velocity vectors, $\boldsymbol{k}$ and $\boldsymbol{k}'$. θ_t represents the scattering angle between the reactant relative velocity and product relative velocity. θ_r and ϕ_r represent the so-called polar and azimuzal angles of the product rotational angular momentum $\boldsymbol{j}'$, respectively. In addition, we give the contour plot of the HOBr PES in Fig. 2. It can be seen that there is a potential well which appears on the exit valley and its existence will influence the dynamics of the title reaction greatly.

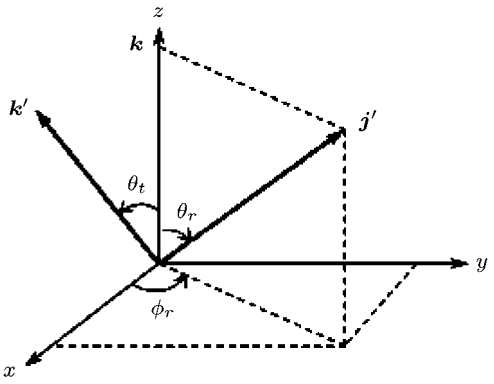


Fig. 1. Centre-of-mass coordinate systerm used to describe the $\boldsymbol{k}$, $\boldsymbol{k}'$, and $\boldsymbol{j}'$ distribution.

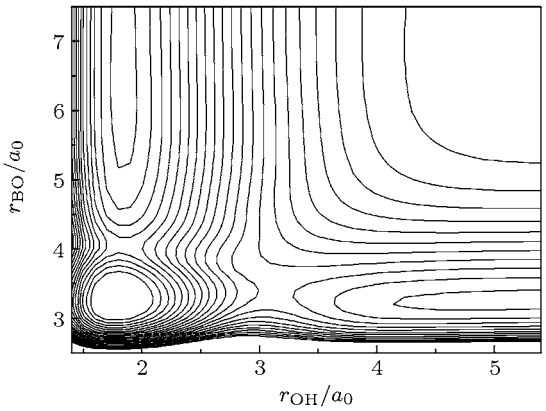


Fig. 2. Contour plot of the HOBr PES for fixed θ (HOBr) at 180°.

The generalized polarization-dependent differential cross sections (PDDCSs) are used to describe the vector correlation of $\boldsymbol{k}$–$\boldsymbol{k}'$–$\boldsymbol{j}'$ and scattering distribution of the product molecule. The $P(\theta_r)$ as a distribution function describing the correlation of $\boldsymbol{k}$–$\boldsymbol{j}'$ can be expanded in a series of Legendre polynomials and the expanding coefficients are called alignment (k is event) and orientation (k is odd) parameters. The $P(\phi_r)$ as a distribution function of the dihedral angle describing $\boldsymbol{k}$–$\boldsymbol{k}'$–$\boldsymbol{j}'$ correlation can be expanded in Fourier series. The $P(\theta_r, \phi_r)$ as a function of angles θ_r and ϕ_r of $\boldsymbol{j}'$ is used to describe the space distribution of the product rotational momentum.

In the CM frame, the fully correlated angular distribution function can be written as the sum,[40] i.e.,

$$P(\omega_t, \omega_r) = \sum_{kq} \frac{[k]}{4\pi} \frac{1}{\sigma} \frac{d\sigma_{kq}}{d\omega_t} C_{kq}(\theta_t, \theta_r)^*, \qquad (1)$$

where $[k] = 2k + 1$ and $(1/\sigma)(d\sigma_{kq}/d\omega_t)$ is the so-called generalized PDDCS. Because many photo-initiated bimolecular reaction experiments are sensitive to those initial polarization moments with

the $k = 0$ and $k = 2$, in this paper, we calculate only $(2\pi/\sigma)\,(\mathrm{d}\sigma_{00}/\mathrm{d}\omega_t)$, $(2\pi/\sigma)\,(\mathrm{d}\sigma_{20}/\mathrm{d}\omega_t)$, $(2\pi/\sigma)\,(\mathrm{d}\sigma_{22+}/\mathrm{d}\omega_t)$, and $(2\pi/\sigma)\,(\mathrm{d}\sigma_{21-}/\mathrm{d}\omega_t)$.

3. Results and discussion

As the rotational angular momentum alignment of the product molecule can be measured from the experiment, we calculate the average rotational alignment factor $\langle \mathrm{P}_2(\boldsymbol{j}' \cdot \boldsymbol{k})\rangle$. Figure 3 shows the dependence of the product rotational alignment on collision energies. It can be seen from the figure that the $\langle \mathrm{P}_2(\boldsymbol{j}' \cdot \boldsymbol{k})\rangle$ values change slightly with the increase of collision energy, suggesting that the degree of alignment is almost invariant when the collision energy increases.

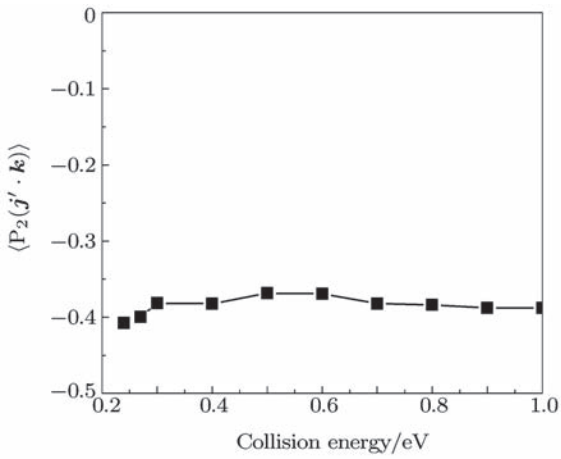


Fig. 3. Product rotational alignment $\langle \mathrm{P}_2(\boldsymbol{j}' \cdot \boldsymbol{k})\rangle$ for $\mathrm{O}(^1\mathrm{D})$+HBr→OH+Br as a function of collision energy.

In order to describe the $\boldsymbol{k}$–$\boldsymbol{j}'$ correlation better than before, we plot the $\mathrm{P}(\theta_r)$ distributions of the product OH in Figs. 4(a) and 4(b). It can be seen from the figure that the $\mathrm{P}(\theta_r)$ distribution is a symmetric distribution with a peak at $\theta_r = 90°$, which indicates that the product rotation angular momentum vector prefers to be perpendicular to the reagent relative velocity. In Fig. 4(a), we can see that the peak value of $\mathrm{P}(\theta_r)$ becomes larger when the collision energy increases from 0.3 eV to 0.4 eV, indicating that the product rotational alignment becomes stronger in this case, while the peak value of $\mathrm{P}(\theta_r)$ becomes smaller when the collision energy increases from 0.4 eV to 0.5 eV, indicating that the product rotational alignment becomes weaker. In addition, it can be found from Fig. 4(b) that the peak value of $\mathrm{P}(\theta_r)$ becomes larger with the collision energy increasing from 0.6 eV to 0.8 eV, implying that the product rotational alignment becomes stronger. Furthermore, from the figure we can obtain another information that the value of $\mathrm{P}(\theta_r)$ is relatively small. As is reported in Refs. [41]–[43], for a reactive system of heavy–light–heavy (HLH) mass combination, the reactant orbital angular momentum $\boldsymbol{L}$ mainly transfers into the product orbital alignment, and $\boldsymbol{j}'$ is almost independent of $\boldsymbol{L}$. In addition, the existing deep well in the exit valley on the PES will lead to a long-life rotating complex for the product channel, and inevitably it will escape from the deep well with weak rotational alignment.

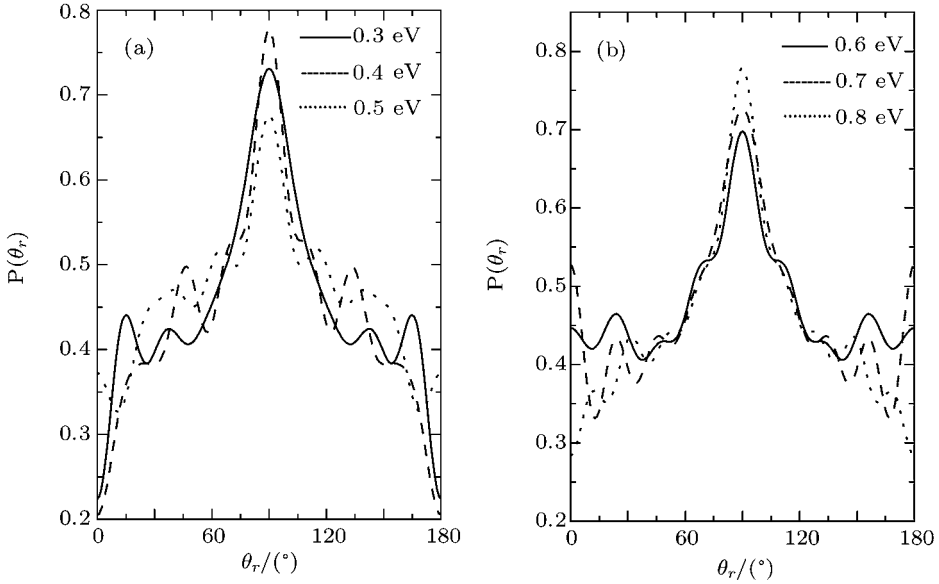


Fig. 4. Distributions of $\mathrm{P}(\theta_r)$ with respect to $\boldsymbol{k}$–$\boldsymbol{j}'$ correlation at six collision energies: (a) $E_\mathrm{c} = 0.3$ eV (solid line), 0.4 eV (dashed line), 0.5 eV (dotted line), and (b) $E_\mathrm{c} = 0.6$ eV (solid line), 0.7 eV (dashed line), 0.8 eV (dotted line).

To obtain a better graphical representation of the product polarization from the title reaction, we plot the distribution $P(\phi_r)$ as a function of dihedral angle to describe the $\boldsymbol{k}$–$\boldsymbol{k}'$–$\boldsymbol{j}'$ correlation in Fig. 6. The $P(\phi_r)$ is not symmetric with respect to the $\boldsymbol{k}$–$\boldsymbol{k}'$ scattering plane, evidently reflecting the polarizations of product rotational angular momentum for six different collision energies. It can be seen in the figure that the $P(\phi_r)$ has two peaks which are at $\phi_r = 90°$ and 270°, separately. It indicates that the rotational angular momentum vector of the product is preferentially aligned along the y axis for the six different collision energies in the CM frame. However, the heights of two peaks are not the same as each other. In general, the peak at $\phi_r = 90°$ is slightly stronger than that at $\phi_r = 270°$, which indicates that the product rotational angular momentum vector is not only aligned but also oriented along the positive y axis. From the figure, we can also see that the value of $P(\phi_r)$ is rather small for the HLH mass combination of the reaction and the deep well on the PES.

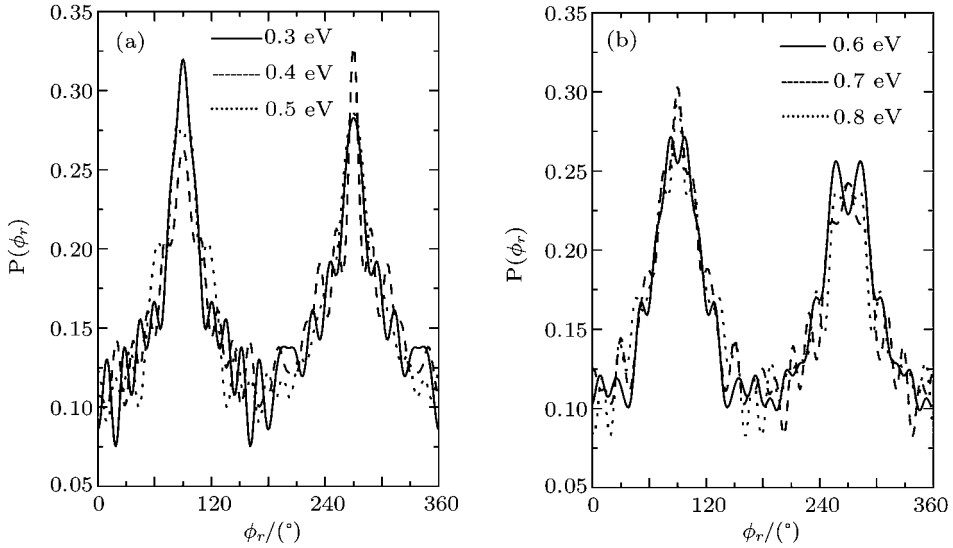


Fig. 5. Dihedral angle distributions of $P(\phi_r)$ with respect to $\boldsymbol{k}$–$\boldsymbol{k}'$ plane at (a) $E_c = 0.3$ eV (solid line), 0.4 eV (dashed line), 0.5 eV (dotted line) and (b) $E_c = 0.6$ eV (solid line), 0.7 eV (dashed line), 0.8 eV (dotted line).

Figure 5(a) shows that the trend that the orientation of the product rotational angular momentum $\boldsymbol{j}'$ changes from the positive y axis to the negative y axis with the collision energy increasing from 0.3 eV to 0.4 eV, while the orientation is along the positive y axis as the collision energy increases from 0.4 eV to 0.5 eV. However, $\boldsymbol{j}'$ is more strongly oriented along the positive y axis with the collision energy increasing from 0.6 eV to 0.8 eV as shown in Fig. 5(b). It can also be seen that the separation between the two peaks is small, implying that the degree of orientation is not very distinct. The distribution of $P(\phi_r)$ tends to be asymmetric with respect to the $\boldsymbol{k}$–$\boldsymbol{k}'$ scattering plane, which may attribute to the effect of the repulsive energy between H–Br atoms. We can derive the expression of the product angular momentum using the "impulsive collision model" of a type A + BC → AB + C reaction developed by Han *et al.*[44] For the reaction O + HBr → OH + Br, the angular momentum $\boldsymbol{j}'$ of the product molecule OH can be written as[34,44,45]

$$j' = L\sin^2\beta + j\cos^2\beta + J_1 m_{\rm H}/m_{\rm OH}, \quad (2)$$

$$\cos^2\beta = \frac{m_{\rm O}\cdot m_{\rm Br}}{(m_{\rm O}+m_{\rm H})(m_{\rm H}+m_{\rm Br})}, \quad (3)$$

$$J_1 = \sqrt{\mu_{\rm HBr}E_{\rm R}}(r_{\rm OH}\times r_{\rm HBr}), \quad (4)$$

where $\boldsymbol{L}$ and $\boldsymbol{j}$ represent the reactant orbital and rotational angular momentum, respectively, $\mu_{\rm HBr}$ is the reduced mass of the HBr molecule, $E_{\rm R}$ is the repulsive energy between H and Br, $r_{\rm OH}$ and $r_{\rm HBr}$ denote unit vectors where the directions of H point to O and Br, respectively. During the processes of chemical-bond forming and breaking of the title reaction, the term $L\sin^2\beta + j\cos^2\beta$ in the equation is symmetric, while the term $J_1 m_{\rm H}/m_{\rm OH}$ is aligned along a direction, owing to the effect of the repulsive energy, which leads the product molecule OH to rotate in a plane parallel to the scattering plane.

In order to provide more detailed information

about the angular momentum polarization of the title reaction, we calculate the distribution of $\mathrm{P}(\theta_r, \phi_r)$ which can be seen in Figs. 6(a)–6(f). From the figure, we can see that $\mathrm{P}(\theta_r, \phi_r)$ has a peak at (90°, 90°) and (90°, 270°), respectively, which are well consistent with the distributions of $\mathrm{P}(\theta_r)$ and $\mathrm{P}(\phi_r)$ of the product OH for six different collision energies. The distribution of $\mathrm{P}(\theta_r, \phi_r)$ indicates that the rotational angular momentum of the product molecule is polarized mainly in the direction perpendicular to the scattering plane. In addition, it also suggests that the product molecule OH is rotating mainly in a plane parallel to the scattering plane.

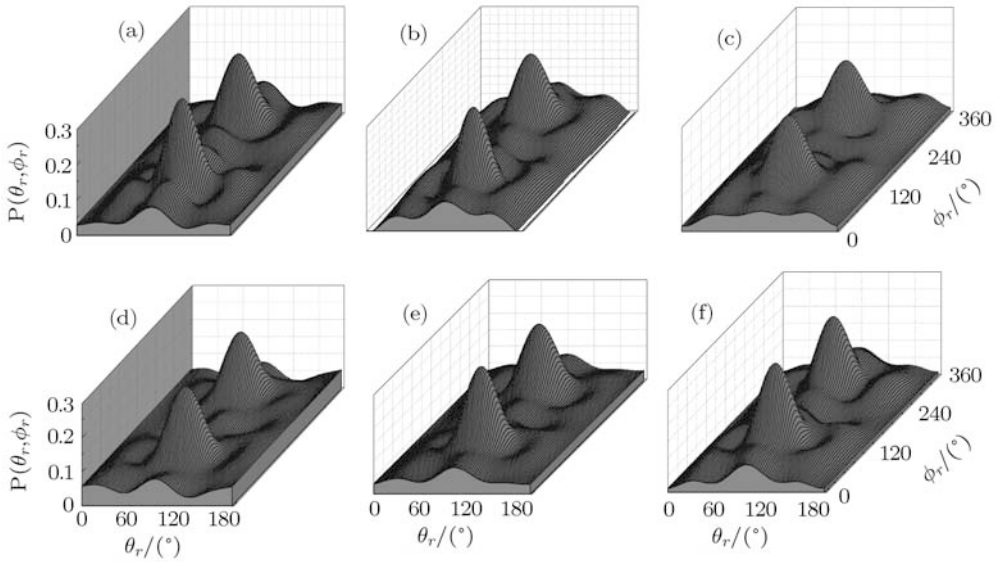


Fig. 6. Polar plots of $\mathrm{P}(\theta_r, \phi_r)$ distribution for six different collision energies averaged over all scattering angles: (a) $E_\mathrm{c} = 0.3$ eV, (b) $E_\mathrm{c} = 0.4$ eV, (c) $E_\mathrm{c} = 0.5$ eV, (d) $E_\mathrm{c} = 0.6$ eV, (e) $E_\mathrm{c} = 0.7$ eV, (f) $E_\mathrm{c} = 0.8$ eV.

To better describe the $\boldsymbol{k}$–$\boldsymbol{k}'$–$\boldsymbol{j}'$ correlation and the scattering direction of the product molecule OH, we calculate the PDDCS for the title reaction on the global adiabatic PES shown in Figs. 7(a)–7(f) corresponding to collision energies 0.3 eV–0.8 eV, respectively. The PDDCS of $(2\pi/\sigma)\,(\mathrm{d}\sigma_{00}/\mathrm{d}\omega_t)$ is dependent only on the scattering angle θ_t but independent of the orientation and the alignment of the product rotational angular momentum vector $\boldsymbol{j}'$. So it reflects the $\boldsymbol{k}$–$\boldsymbol{k}'$ correlation or the angular distribution of the product. As shown in Fig. 7, the product molecule OH is scattered strongly forward. The PDDCS of $(2\pi/\sigma)\,(\mathrm{d}\sigma_{20}/\mathrm{d}\omega_t)$ is related to not only scattering angle θ_t but also $\langle 3\cos^2\theta_r - 1\rangle$. So it is called the average value of the second Legendre moment $\langle P_2(\cos\theta_r)\rangle$. From the figure, it is obvious that the trend of the $(2\pi/\sigma)\,(\mathrm{d}\sigma_{20}/\mathrm{d}\omega_t)$ is opposite to that of the $(2\pi/\sigma)\,(\mathrm{d}\sigma_{00}/\mathrm{d}\omega_t)$, indicating that the value of $\langle 3\cos^2\theta_r - 1\rangle$ is negative or the alignment of the product molecule rotational angular momentum $\boldsymbol{j}'$ is perpendicular to $\boldsymbol{k}$.

In addition, we can also see in Fig. 7 that the PDDCSs with $q \neq 0$ are zero when the values of scattering angle θ_t are 0° and 180°. Because the $\boldsymbol{k}$–$\boldsymbol{k}'$ scattering plane is uncertain at these limiting scattering angles, the values of these PDDCSs must be zero. From the figure, it is easy to see that the values of $(2\pi/\sigma)\,(\mathrm{d}\sigma_{22+}/\mathrm{d}\omega_t)$ are negative in the whole range of scattering angle θ_t, implying that the product alignment is along the y axis. It is noticeable that the product exhibits a stronger polarization when θ_t is near 30°, which is similar to the result in Ref. [46]. We can also know that the PDDCS of $(2\pi/\sigma)\,(\mathrm{d}\sigma_{21-}/\mathrm{d}\omega_t)$ is different from that of other reactions. The values of the $(2\pi/\sigma)\,(\mathrm{d}\sigma_{21-}/\mathrm{d}\omega_t)$ are negative when the scattering angle θ_t is less than 40°, which suggests that the product is aligned along the direction of $\boldsymbol{x} + \boldsymbol{z}$. The values of the $(2\pi/\sigma)\,(\mathrm{d}\sigma_{21-}/\mathrm{d}\omega_t)$ are positive when the scattering angle θ_t is in a range from 40° to 180°, suggesting that the product alignment is along the direction of $\boldsymbol{x} - \boldsymbol{z}$.

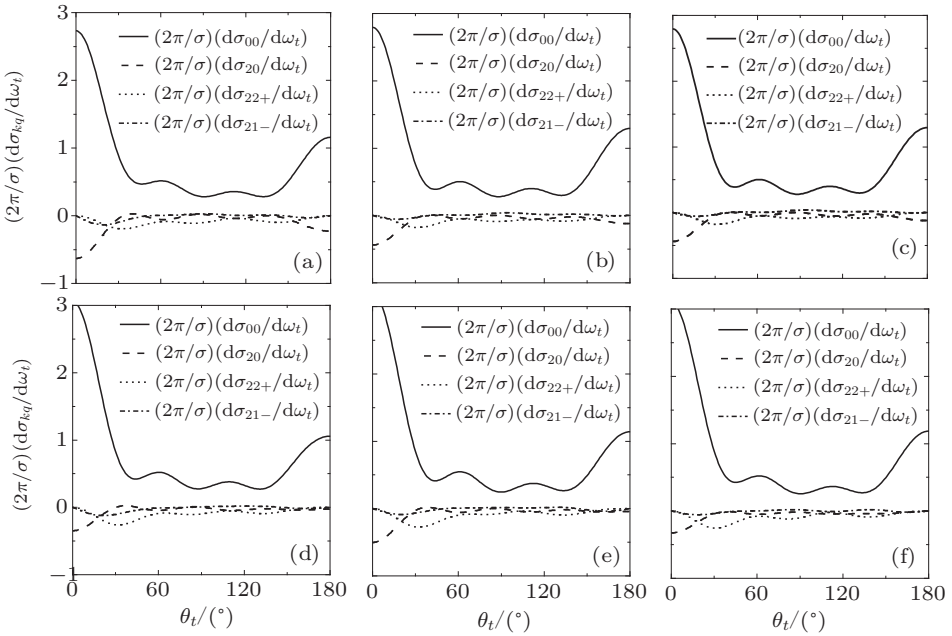


Fig. 7. Polarization-dependent generalized differential cross sections of the title reaction for six different collision energies. Solid line indicates $(2\pi/\sigma)\,(\mathrm{d}\sigma_{00}/\mathrm{d}\omega_t)$, dashed line indicates $(2\pi/\sigma)\,(\mathrm{d}\sigma_{20}/\mathrm{d}\omega_t)$, dotted line indicates $(2\pi/\sigma)\,(\mathrm{d}\sigma_{22+}/\mathrm{d}\omega_t)$ and short dash-dotted line indicates $(2\pi/\sigma)\,(\mathrm{d}\sigma_{21-}/\mathrm{d}\omega_t)$. (a) $E_\mathrm{c} = 0.3$ eV, (b) $E_\mathrm{c} = 0.4$ eV, (c) $E_\mathrm{c} = 0.5$ eV, (d) $E_\mathrm{c} = 0.6$ eV, (e) $E_\mathrm{c} = 0.7$ eV, (f) $E_\mathrm{c} = 0.8$ eV.

4. Conclusion

In this paper, the product polarizations of the title reaction at different collision energies are analysed by using the QCT method. The rotational angular momentum vector $\boldsymbol{j}'$ of the product molecule OH is strongly aligned and slightly oriented along the positive y axis. The four PDDCSs display that the product molecule OH tends mainly to the forward scattering and the trend of forward scattering becomes stronger with the increase of collision energy. Due to the type of HLH mass combination and the deep potential well on the PES, the alignment and the orientation degrees of the product rotational angular momentum vector $\boldsymbol{j}'$ are relatively weak. These results obtained from our work are probably helpful for exploring the similar reactions and providing some useful information for the future relevant experiments.

References

[1] González-Sánchez L, Gómez-Carrasco S and Aguado A 2004 *J. Chem. Phys.* **121** 309

[2] Gómez-Carrasco S, González-Sánchez L and Aguado A 2004 *J. Chem. Phys.* **121** 4605

[3] Gómez-Carrasco S, González-Sánchez L and Aguado A 2004 *Chem. Phys. Lett.* **383** 25

[4] Gómez-Carrasco S, Roncero O and González-Sánchez L 2005 *J. Chem. Phys.* **123** 114310

[5] Gómez-Carrasco S, Aguado A, Paniagua M and Roncero O 2007 *J. Photochem. Photobiol.* A **190** 145

[6] Gómez-Carrasco S, Hernándezb M L and Alvariño J M 2007 *Chem. Phys. Lett.* **435** 188

[7] González-Sánchez L, Gómez-Carrasco S, Aguado A, Paniagua M, Hernández M L, Alvariño J M and Roncero O 2004 *Mol. Phys.* **102** 2381

[8] Yung Y L, Pinto J P, Watson R T and Sander S P 1980 *J. Atoms. Sci.* **37** 39

[9] Garcia R R and Solomon S 1994 *J. Geophys. Res.* **99** 12397

[10] Orlando J J and Burkholder J B 1995 *J. Phys. Chem.* **99** 1143

[11] Benter T, Feldman C, Kirchner U, Schmidt M, Schmidt S, Schindler R N and Bunsenges B 1995 *Phys. Chem.* **99** 1144

[12] Barnes R J, Lock M, Coleman J and Sinha A 1996 *J. Phys. Chem.* **100** 453

[13] Deters B, Himmelmann S, Blindauer C and Burrows J P 1996 *Ann. Geophys.* **14** 468

[14] Rattigan O V, Lary D J, Jones R L and Cox R A 1996 *J. Geophys. Res.* **101** 23021

[15] Ingham T, Bauer D, Landgraf J and Crowley J N 1998 *J. Phys. Chem.* **102** 3293

[16] Ruscic B and Berkowitz J 1994 *J. Chem. Phys.* **101** 7795

[17] Lock M, Barnes R J and Sinha A 1996 *J. Phys. Chem.* **100** 7972

[18] McGrath M P and Rowland F S 1994 *J. Phys. Chem.* **98** 4773

[19] Palmieri P, Puzzarini C and Tarroni R 1996 *Chem. Phys. Lett.* **256** 409

[20] Peterson K A 1997 *Spectrochim. Acta* A **53** 1051

[21] Lee T J 1995 *J. Phys. Chem.* **99** 15074

[22] Lee T J, Parthiban S and Head-Gordan M 1999 *Spectrochim. Acta* A **55** 561

[23] Füsti-Molnar L, Szalay P G and Balint-Kurti G G 1999 *J. Chem. Phys.* **110** 8448

[24] Peterson K A 2000 *J. Chem. Phys.* **113** 4598

[25] Tang B Y, Tang Q K, Chen M D, Han K L and Zhang J Z 2004 *J. Chem. Phys.* **120** 8537

[26] Gogtas F 2006 *Chem. Phys.* **328** 421

[27] Skokov S, Peterson K A and Bowman J M 1998 *J. Chem. Phys.* **109** 2662

[28] Peterson K A, Skokov S and Bowman J M 1999 *J. Chem. Phys.* **111** 7446

[29] Han K L, He G Z and Lou N Q 1996 *J. Chem. Phys.* **105** 8699

[30] Wang M L, Han K L and He G Z 1998 *J. Chem. Phys.* A **102** 10204

[31] Chen M D, Han K L and Lou N Q 2003 *J. Chem. Phys.* **118** 4463

[32] Wang M L, Han K L and He G Z 1998 *J. Chem. Phys.* **109** 5446

[33] Zhang X and Han K L 2006 *Int. J. Quantum Chem.* **106** 1815

[34] Chen M D, Han K L and Lou N Q 2002 *Chem. Phys. Lett.* **357** 483

[35] Fu Y B, Luo W L, Ruan W, Zhang L and Zhu Z H 2009 *Chin. Phys.* B **18** 167

[36] Zhao J, Xu Y and Meng Q T 2010 *Chin. Phys.* B **19** 063403

[37] Zhao J and Luo Y 2010 *Chin. Phys.* B **20** 043402

[38] Xu Y, Zhao J, Wang J, Liu F and Meng Q T 2010 *Acta Phys. Sin.* **59** 638 (in Chinese)

[39] Han K L, He G Z and Lou N Q 1993 *Chin. Chem. Lett.* **4** 517

[40] Aoiz F J, Brouard M and Enriquez P A 1996 *J. Chem. Phys.* **105** 4964

[41] Wang M L, Han K L and He G Z 1998 *J. Chem. Phys.* **102** 10204

[42] Han K L, He G Z and Lou N Q 1996 *J. Chem. Phys.* **105** 8699

[43] Wang M L, Han K L and He G Z 1998 *J. Chem. Phys.* **109** 5446

[44] Han K L, He G Z and Lou N Q 1989 *Chin. J. Chem. Phys.* **2** 323

[45] Li R J, Han K L, Li F E, Lu R C, He G Z and Lou N Q 1994 *Chem. Phys. Lett.* **220** 286

[46] Xu Y, Zhao J, Yue D G, Liu H, Zheng X Y and Meng Q T 2009 *Chin. Phys.* B **18** 5308